

Electronic Supplementary Information

Bimetallic MOF-based catalysts with enhanced activity for electrochemical hydrogen evolution in acid and alkaline electrolytes

Rui-Zhe Zhang^{a,b*}, Lele Lu^a, Peng Cheng^a and Wei Shi^{a*}

^aFrontiers Science Center for New Organic Matter, Key Laboratory of Advanced Energy Materials Chemistry (MOE), State Key Laboratory of Advanced Chemical Power Sources, College of Chemistry, Nankai University, Tianjin 300071, China

^bSchool of Chemistry and Pharmaceutical Engineering, Shandong First Medical University & Shandong Academy of Medical Sciences, Jinan 250000, China

Contents

Table S1	MOF-based HER electrocatalysts applied in acidic electrolyte.	S3
Table S2	MOF-based HER electrocatalysts applied in alkaline electrolyte.	S4
Fig. S1	Thermogravimetric analysis of Ni-NKU-100 and M_xNi_{1-x} -NKU-100 (M = Mn, Fe, Co, Cu, Zn).	S5
Fig. S2	SEM images of Ni-NKU-100, $Cu_{0.16}Ni_{0.84}$ -NKU-100 and $Fe_{0.24}Ni_{0.76}$ -NKU-100.	S6
Fig. S3	SEM images and EDS elemental mappings of $Mn_{0.14}Ni_{0.86}$ -NKU-100 (a), $Fe_{0.24}Ni_{0.76}$ -NKU-100 (b), $Co_{0.18}Ni_{0.82}$ -NKU-100 (c), $Cu_{0.16}Ni_{0.84}$ -NKU-100 (d), and $Zn_{0.18}Ni_{0.82}$ -NKU-100 (e).	S7
Fig. S4	LSV curves and EIS Nyquist plots of M_xNi_{1-x} -NKU-100 (M = Mn, Fe, Co, Cu, Zn) in 0.5 M H_2SO_4 electrolyte.	S8
Fig. S5	The equivalent circuit for fitting electrochemical impedance.	S9
Table S3	R_{ct} of Cu_xNi_{1-x} -NKU-100 in 0.5 M H_2SO_4 electrolyte.	S10
Fig. S6	CV curves of Ni-NKU-100 and Cu_xNi_{1-x} -NKU-100 at the scan rate range from 20 to 200 $mV s^{-1}$ in 0.5 M H_2SO_4 electrolyte.	S11
Fig. S7	SEM images of $Cu_{0.22}Ni_{0.78}$ -NKU-100 after long-time electrocatalytic test in 0.5 M H_2SO_4 electrolyte.	S12
Fig. S8	XPS wide spectra for Ni-NKU-100 and Cu_xNi_{1-x} -NKU-100.	S13
Fig. S9	High-resolution XPS of Ni 2p for Cu_xNi_{1-x} -NKU-100.	S14
Fig. S10	High-resolution XPS of Cu 2p for Cu_xNi_{1-x} -NKU-100.	S15
Fig. S11	High-resolution XPS of C 1s for Cu_xNi_{1-x} -NKU-100.	S16
Fig. S12	High-resolution XPS of O 1s for Cu_xNi_{1-x} -NKU-100.	S17
Fig. S13	LSV curves and EIS Nyquist plots of M_xNi_{1-x} -NKU-100 (M = Mn, Fe, Co, Cu, Zn) in 1 M NaOH electrolyte.	S18
Fig. S14	CV curves of Ni-NKU-100 and Fe_xNi_{1-x} -NKU-100 at the scan rate range from 20 to 200 $mV s^{-1}$ in 1 M NaOH electrolyte.	S19
Table S4	R_{ct} of Fe_xNi_{1-x} -NKU-100 in 1 M NaOH electrolyte.	S20
Fig. S15	SEM images of $Fe_{0.24}Ni_{0.76}$ -NKU-100 after long-time electrocatalytic test in 1 M NaOH electrolyte.	S21
Fig. S16	XPS wide spectra for Ni-NKU-100 and Cu_xNi_{1-x} -NKU-100.	S22
Fig. S17	High-resolution XPS of Ni 2p for Fe_xNi_{1-x} -NKU-100.	S23
Fig. S18	High-resolution XPS of Fe 2p for Fe_xNi_{1-x} -NKU-100.	S24
Fig. S19	High-resolution XPS of C 1s for Fe_xNi_{1-x} -NKU-100.	S25
Fig. S20	High-resolution XPS of O 1s for Fe_xNi_{1-x} -NKU-100.	S26
References		S27

Table S1. MOF-based HER electrocatalysts applied in acidic electrolyte.

Catalysts	Categories	η_{10} (mV)	Electrolyte	Stability	Reference
Ni-NKU-100	3D MOF	224	0.5 M H ₂ SO ₄	24 h	This work
Cu _{0.22} Ni _{0.78} -NKU-100					
Co-MOF	3D MOF	357	0.5 M H ₂ SO ₄	96 h	[1]
Co-MOF	3D MOF	223	0.5 M H ₂ SO ₄	72 h	[2]
THAT-Co-single layer		283			
THTA-Co-powder	2D MOF	332	0.5 M H ₂ SO ₄	4 h	[3]
THTA-Co-graphene		230			
CTGU-9	3D MOF	424	0.5 M H ₂ SO ₄	21 h	[4]
AB: CTGU-9=3: 4					
UU-100(Co)	3D MOF	450	NaClO ₄ (0.1 M)/ acetate (0.2 M) buffer at pH 4	~5 h	[5]
THT-Ni	2D MOF	333	0.5 M H ₂ SO ₄		[6]
Cu-MOF	3D MOF	440	1 M H ₂ SO ₄		[7]
NENU-5		585			
HKUST-1		691			
NENU-500	3D MOF	237	0.5 M H ₂ SO ₄		[8]
NENU-501		392			
NENU-499		570			
$\epsilon(\text{trim})_{4/3}$		515			
NU-1000	3D MOF	640			
NU-1000_Ni-S	3D MOF + sulfide	238	0.1 M HCl	2 h	[9]
bulk NiFe-MOF		196			
HKUST-1 ED	3D MOF	590	0.5 M H ₂ SO ₄	2 h	[10]
HKUST-1 HT		660			
Ni-NKU-100	3D MOF	324	0.5 M H ₂ SO ₄	24 h	[11]
Cu _{0.19} Ni _{0.81} -NKU-101					

Table S2. MOF-based HER electrocatalysts applied in alkaline electrolyte.

Catalysts	Categories	η_{10} (mV)	Electrolyte	Stability	Reference
Ni-NKU-100	3D MOF	249	1 M KOH	24 h	This work
Fe _{0.24} Ni _{0.76} -NKU-100					
Co-BDC	2D MOF	529	1 M KOH	15 h	[12]
Co-BDC-MoS ₂	2D MOF + sulfide	248			
NiFe-MOF	3D MOF	134	0.1 M KOH	5.5 h	[13]
Ni-MOF		177			
bulk NiFe-MOF		196			
Co-BTC/CC	3D MOF	437	1 M KOH		[14]
CuCo-CAT	3D MOF	52	1 M KOH	10 h	[15]
Fe(OH) _x @Cu-MOF	3D MOF	112	1 M KOH	30 h	[16]
Fe ₂ Zn-MOF	3D MOF	221	0.1 M KOH	24 h	[17]
Ni ₃ (Ni ₃ -HAHATN) ₂	3D MOF	115	0.1 M KOH	10 h	[18]

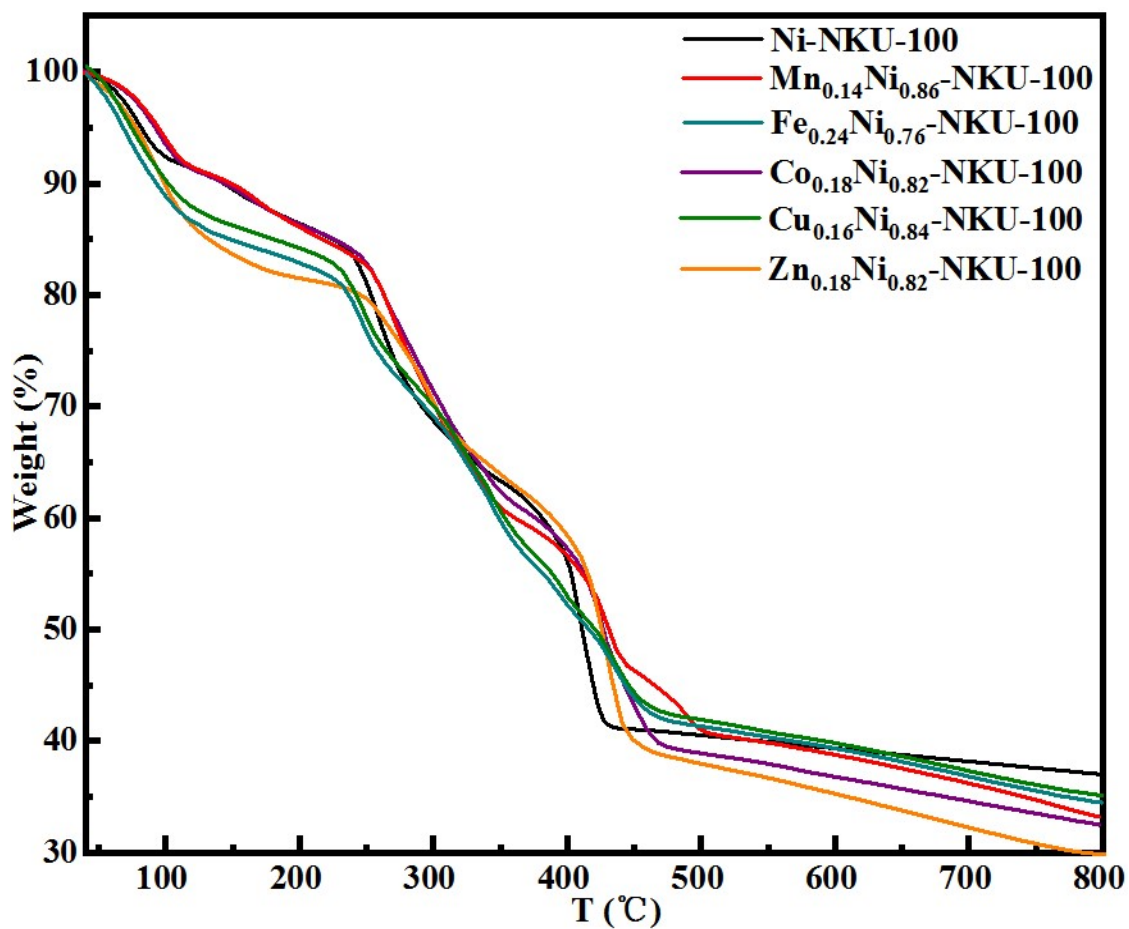


Fig. S1 Thermogravimetric analysis of Ni-NKU-100 and M_xNi_{1-x} -NKU-100 (M = Mn, Fe, Co, Cu, Zn).

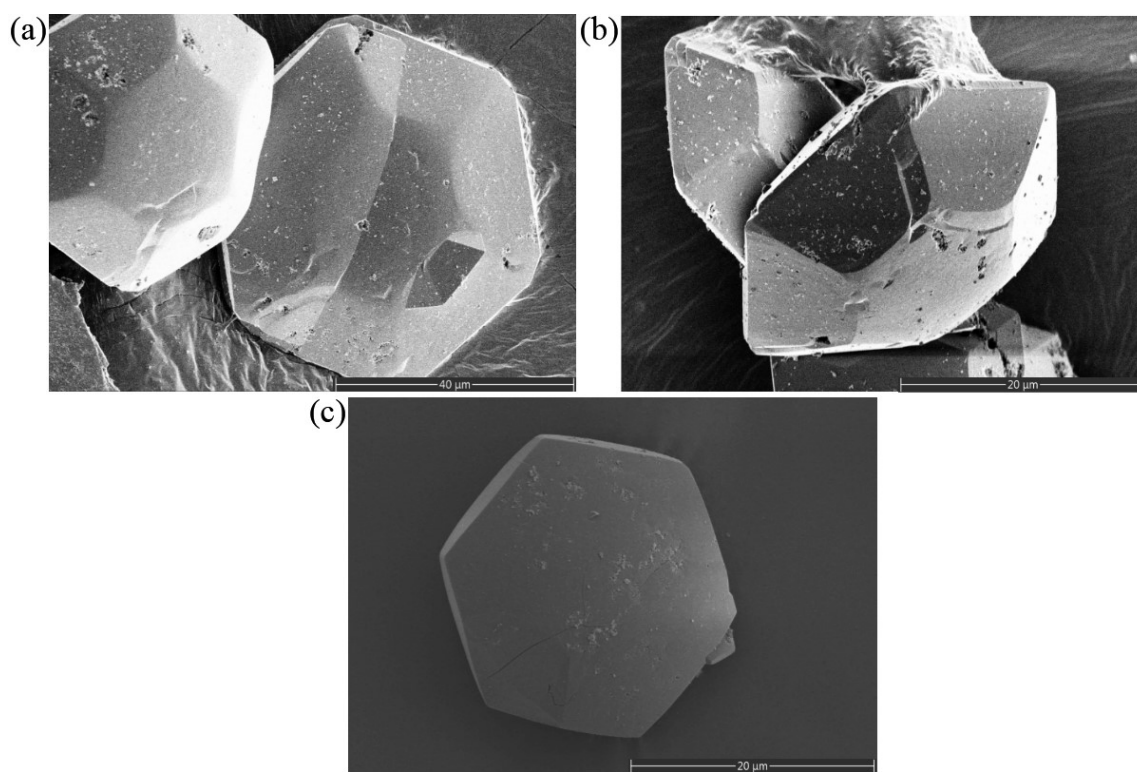


Fig. S2 FESEM images of Ni-NKU-100 (a), $\text{Cu}_{0.16}\text{Ni}_{0.84}\text{-NKU-100}$ (b) and $\text{Fe}_{0.24}\text{Ni}_{0.76}\text{-NKU-100}$ (c).

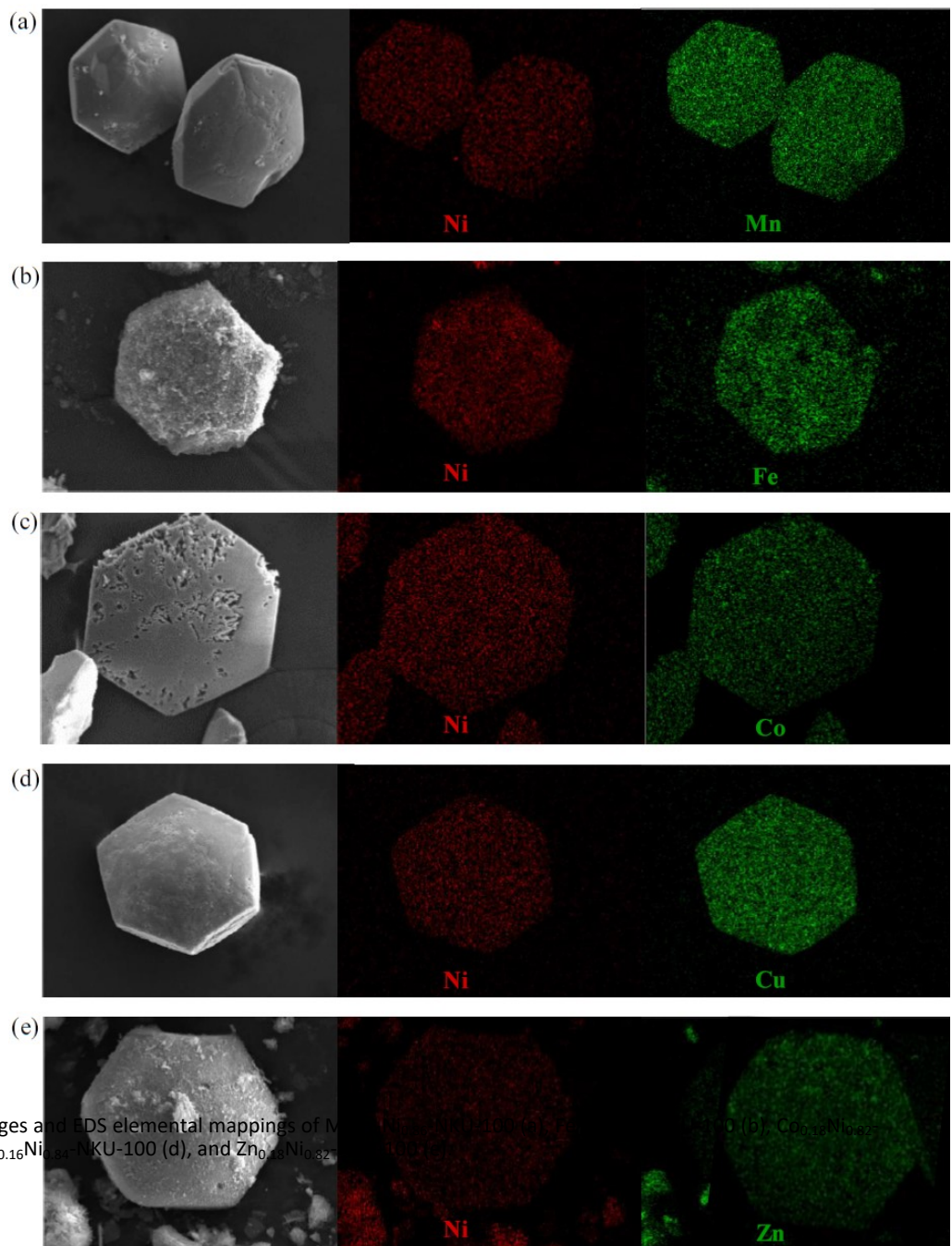


Fig. S3 SEM images and EDS elemental mappings of $\text{Ni}_{0.16}\text{Ni}_{0.16}\text{Ni}_{0.16}\text{-NiKU-100}$ (a), $\text{Cu}_{0.16}\text{Ni}_{0.16}\text{Ni}_{0.16}\text{-NiKU-100}$ (b), $\text{Cu}_{0.16}\text{Ni}_{0.16}\text{Ni}_{0.16}\text{-NiKU-100}$ (c), $\text{Cu}_{0.16}\text{Ni}_{0.16}\text{Ni}_{0.16}\text{-NiKU-100}$ (d), and $\text{Zn}_{0.16}\text{Ni}_{0.16}\text{Ni}_{0.16}\text{-NiKU-100}$ (e).

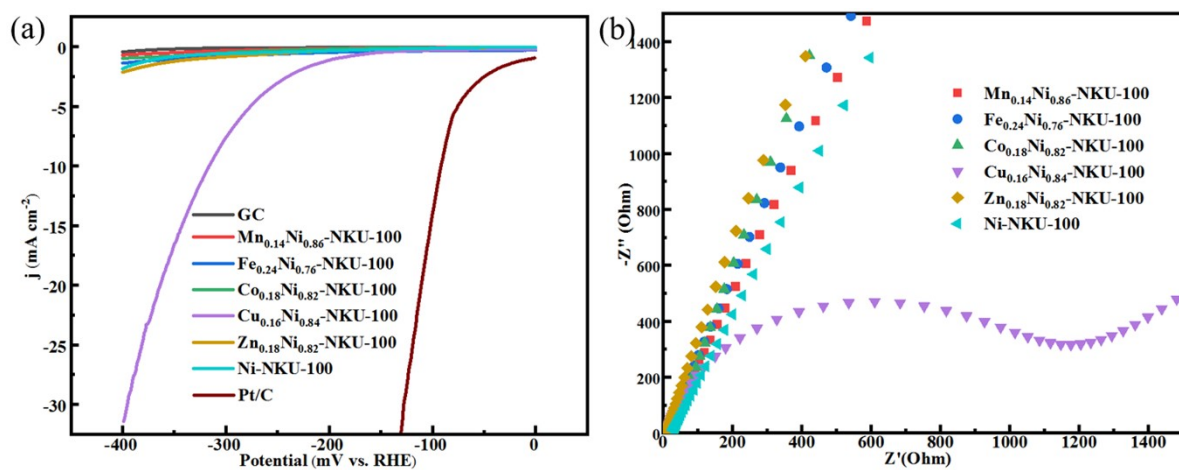


Fig. S4 (a) LSV curves at a scan rate of 5 mV·s⁻¹ and (b) EIS Nyquist plots of M_xNi_{1-x}-NKU-100 (M = Mn, Fe, Co, Cu, Zn) in 0.5 M H₂SO₄ electrolyte.

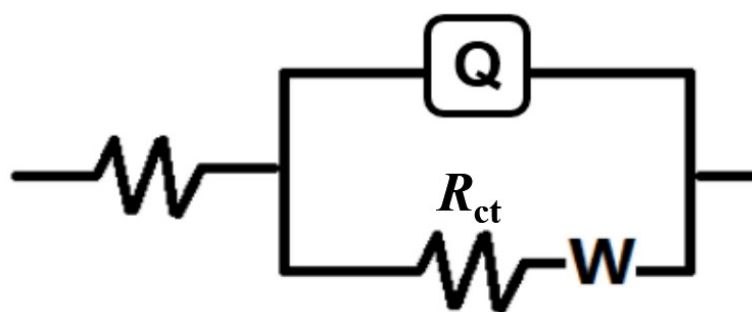
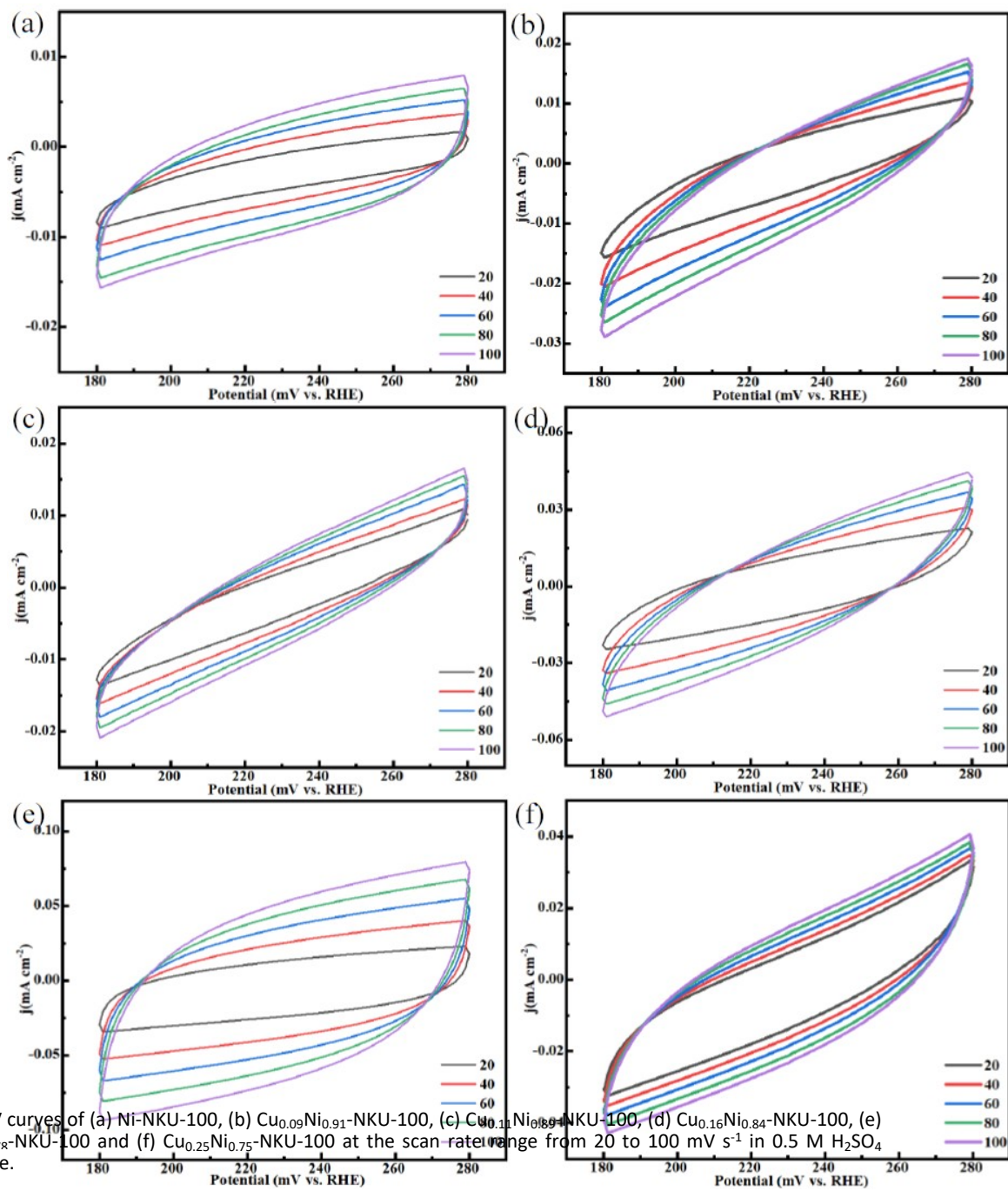


Fig. S5 The equivalent circuit for fitting electrochemical impedance.

Table S3 R_{ct} of $\text{Cu}_x\text{Ni}_{1-x}$ -NKU-100 in 0.5 M H_2SO_4 electrolyte.

Electrode material	R_{ct} (Ω)
Ni-NKU-100	86500
$\text{Cu}_{0.09}\text{Ni}_{0.91}$ -NKU-100	53400
$\text{Cu}_{0.11}\text{Ni}_{0.89}$ -NKU-100	3729
$\text{Cu}_{0.16}\text{Ni}_{0.84}$ -NKU-100	2768
$\text{Cu}_{0.22}\text{Ni}_{0.78}$ -NKU-100	702
$\text{Cu}_{0.25}\text{Ni}_{0.75}$ -NKU-100	1066



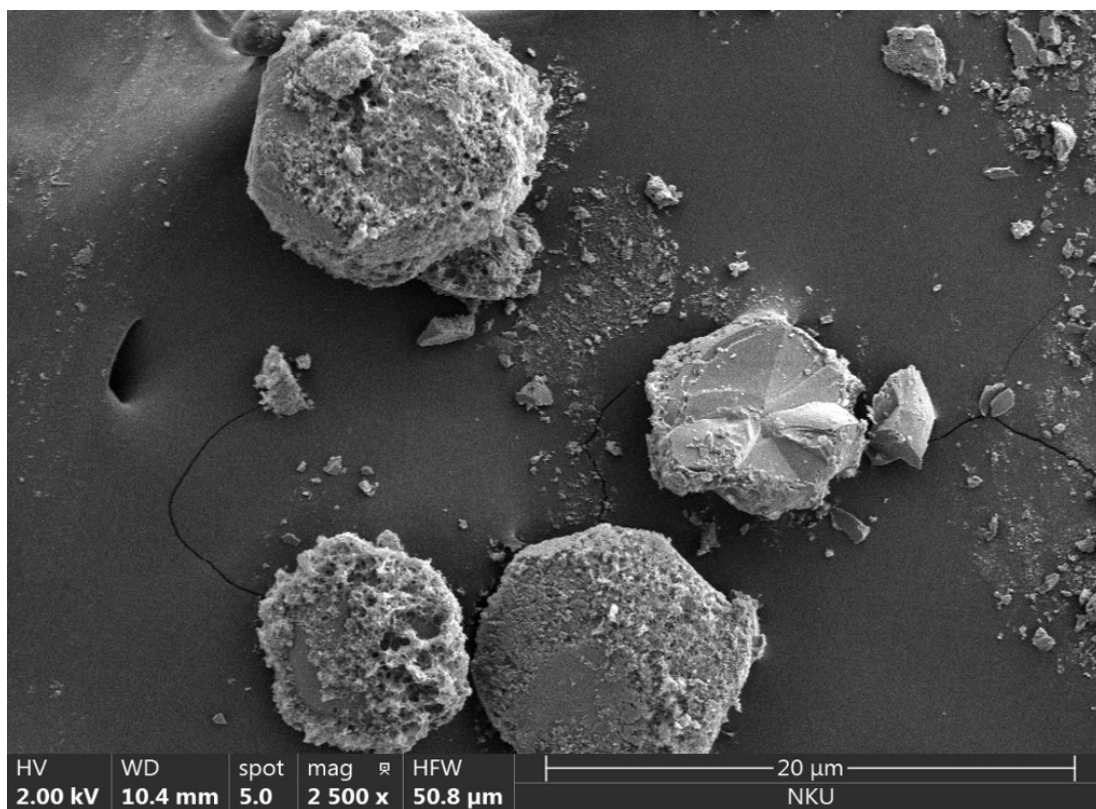


Fig. S7 SEM images of $\text{Cu}_{0.22}\text{Ni}_{0.78}\text{-NKU-100}$ after long-time electrocatalytic test in $0.5 \text{ M H}_2\text{SO}_4$ electrolyte.

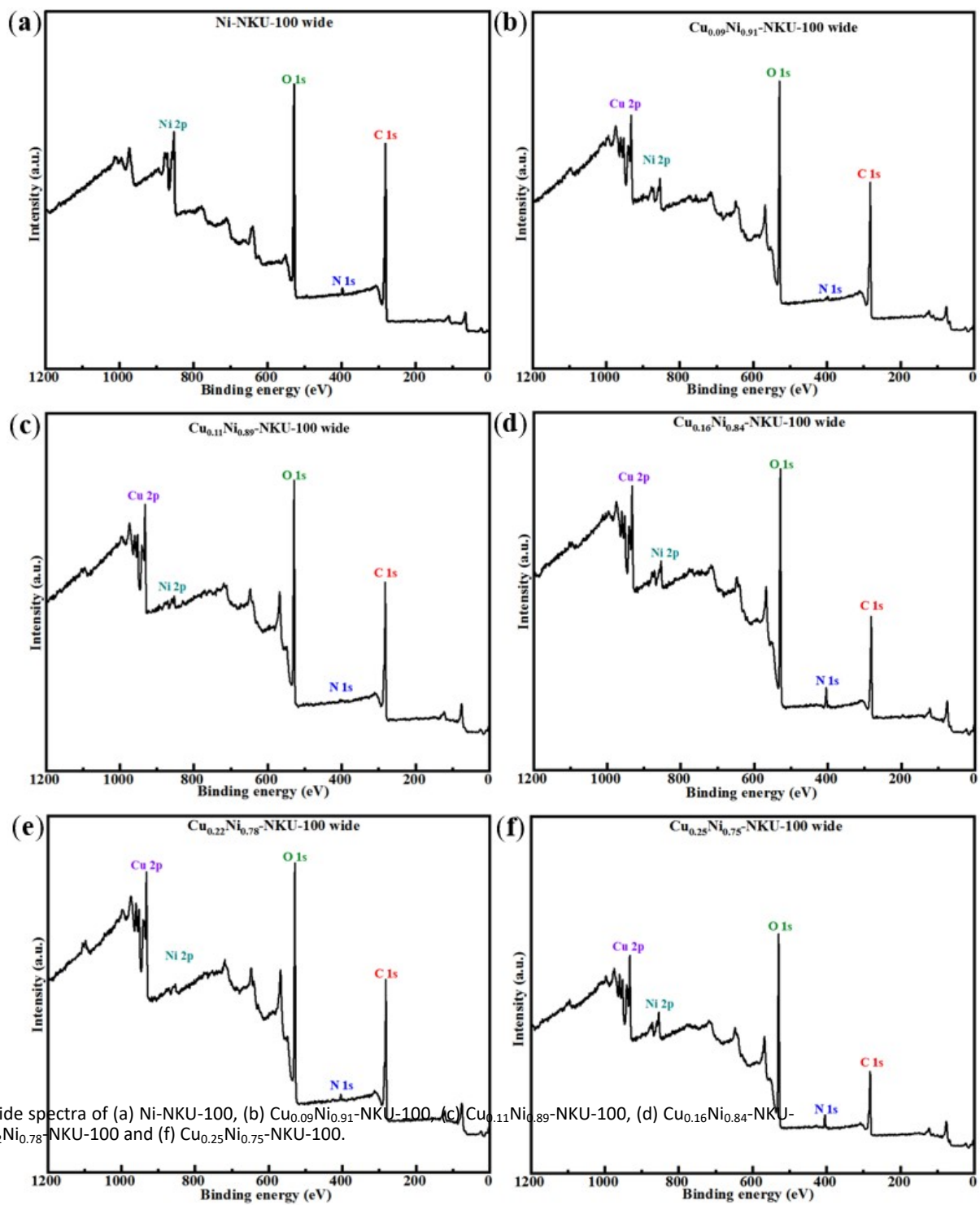


Fig. S8 XPS wide spectra of (a) Ni-NKU-100, (b) $\text{Cu}_{0.09}\text{Ni}_{0.91}$ -NKU-100, (c) $\text{Cu}_{0.11}\text{Ni}_{0.89}$ -NKU-100, (d) $\text{Cu}_{0.16}\text{Ni}_{0.84}$ -NKU-100, (e) $\text{Cu}_{0.22}\text{Ni}_{0.78}$ -NKU-100 and (f) $\text{Cu}_{0.25}\text{Ni}_{0.75}$ -NKU-100.

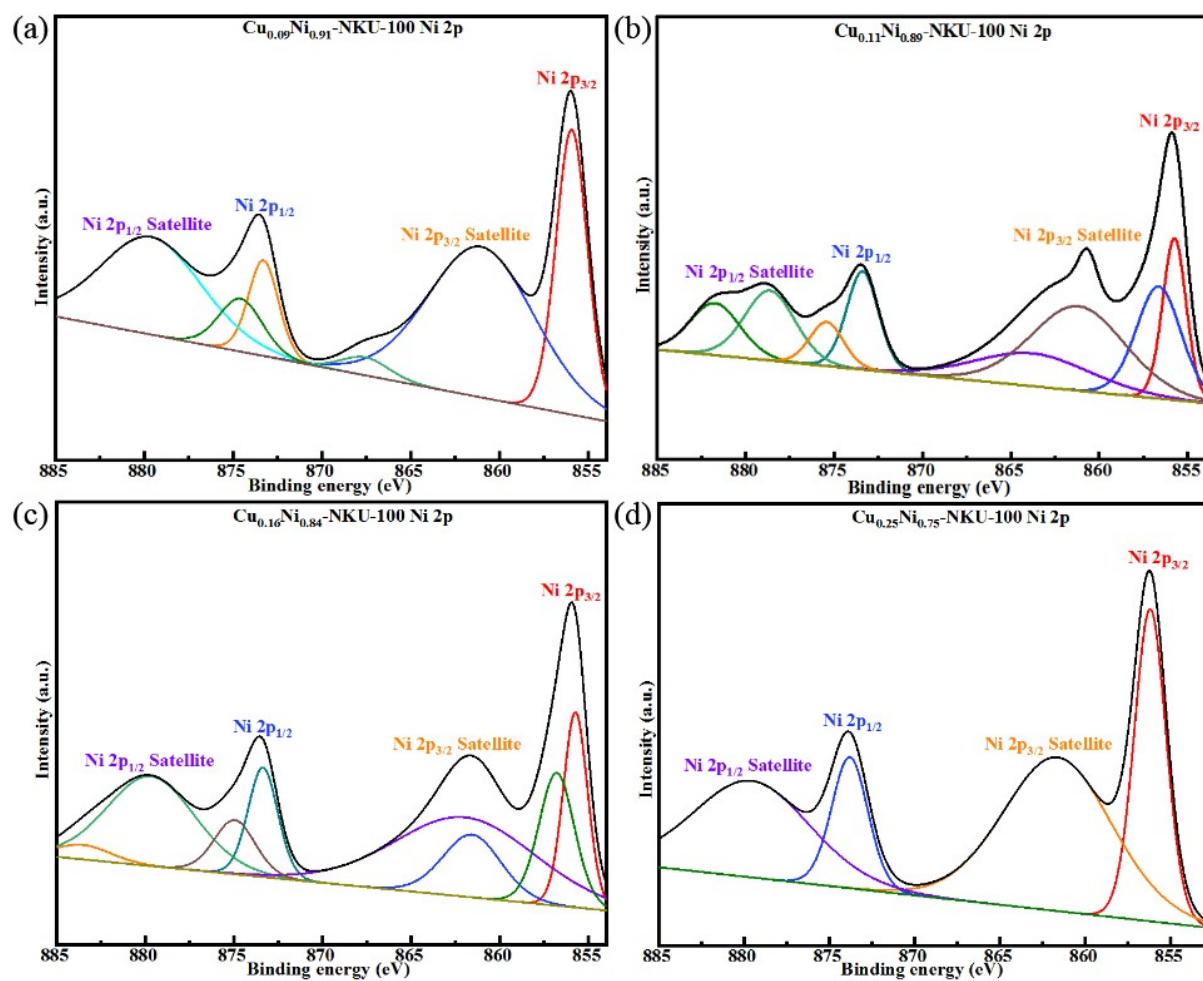


Fig. S9 High-resolution XPS of Ni 2p for (a) $\text{Cu}_{0.09}\text{Ni}_{0.91}\text{-NKU-100}$, (b) $\text{Cu}_{0.11}\text{Ni}_{0.89}\text{-NKU-100}$, (c) $\text{Cu}_{0.16}\text{Ni}_{0.84}\text{-NKU-100}$ and (d) $\text{Cu}_{0.25}\text{Ni}_{0.75}\text{-NKU-100}$.

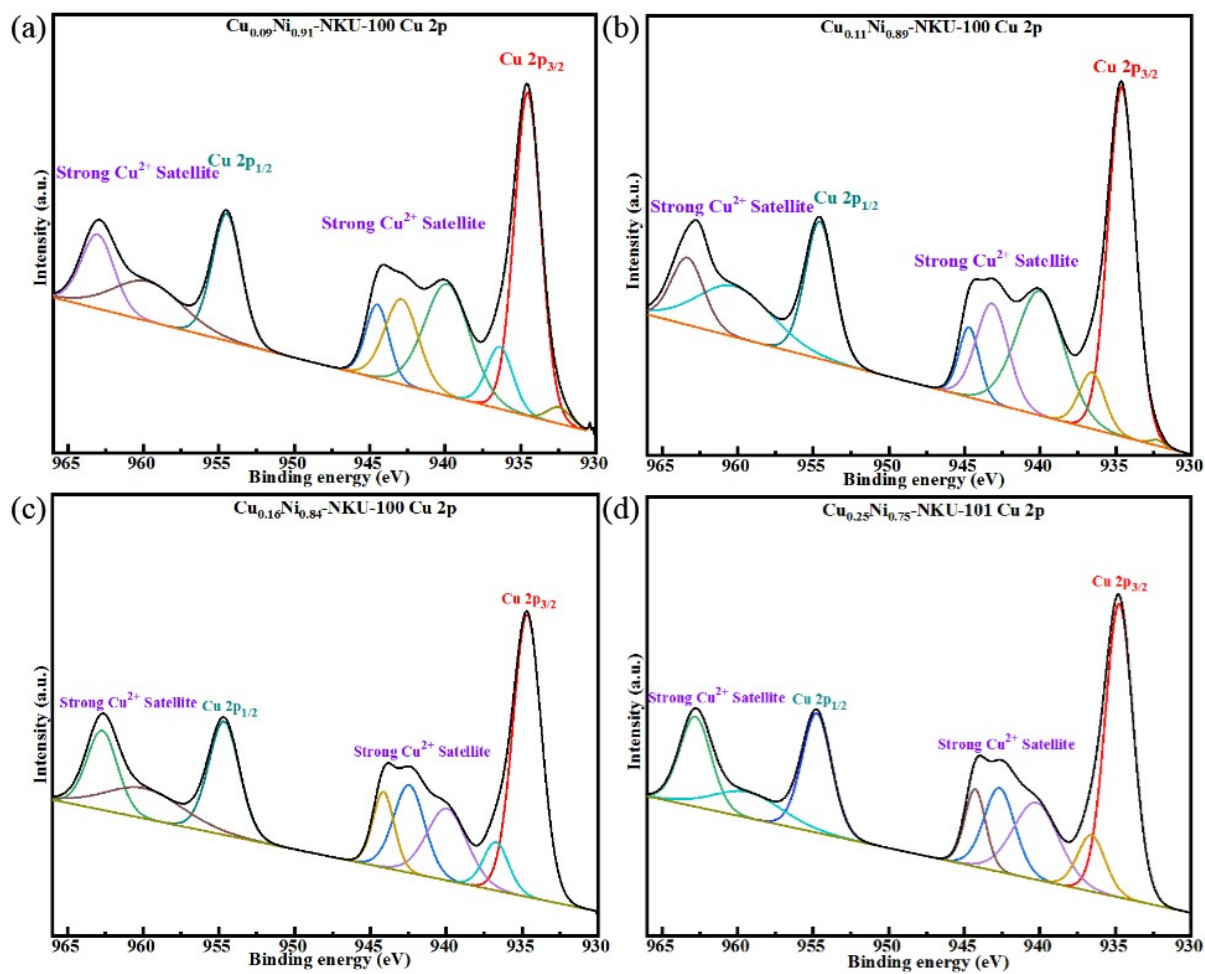


Fig. S10 High-resolution XPS of Cu 2p for (a) $\text{Cu}_{0.09}\text{Ni}_{0.91}\text{-NKU-100}$, (b) $\text{Cu}_{0.11}\text{Ni}_{0.89}\text{-NKU-100}$, (c) $\text{Cu}_{0.16}\text{Ni}_{0.84}\text{-NKU-100}$ and (d) $\text{Cu}_{0.25}\text{Ni}_{0.75}\text{-NKU-100}$.

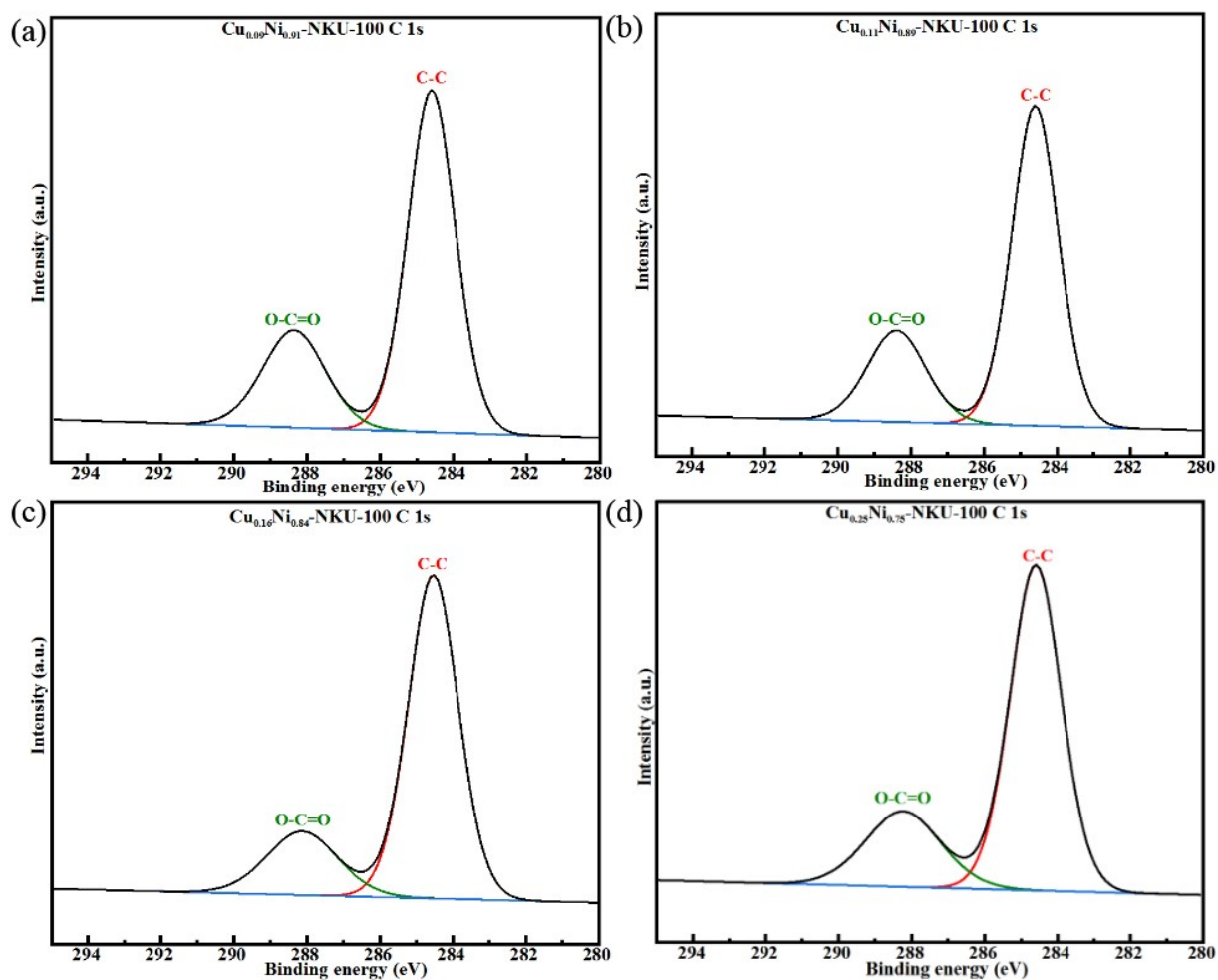


Fig. S11 High-resolution XPS of C 1s for (a) $\text{Cu}_{0.09}\text{Ni}_{0.91}\text{-NKU-100}$, (b) $\text{Cu}_{0.11}\text{Ni}_{0.89}\text{-NKU-100}$, (c) $\text{Cu}_{0.16}\text{Ni}_{0.84}\text{-NKU-100}$ and (d) $\text{Cu}_{0.25}\text{Ni}_{0.75}\text{-NKU-100}$.

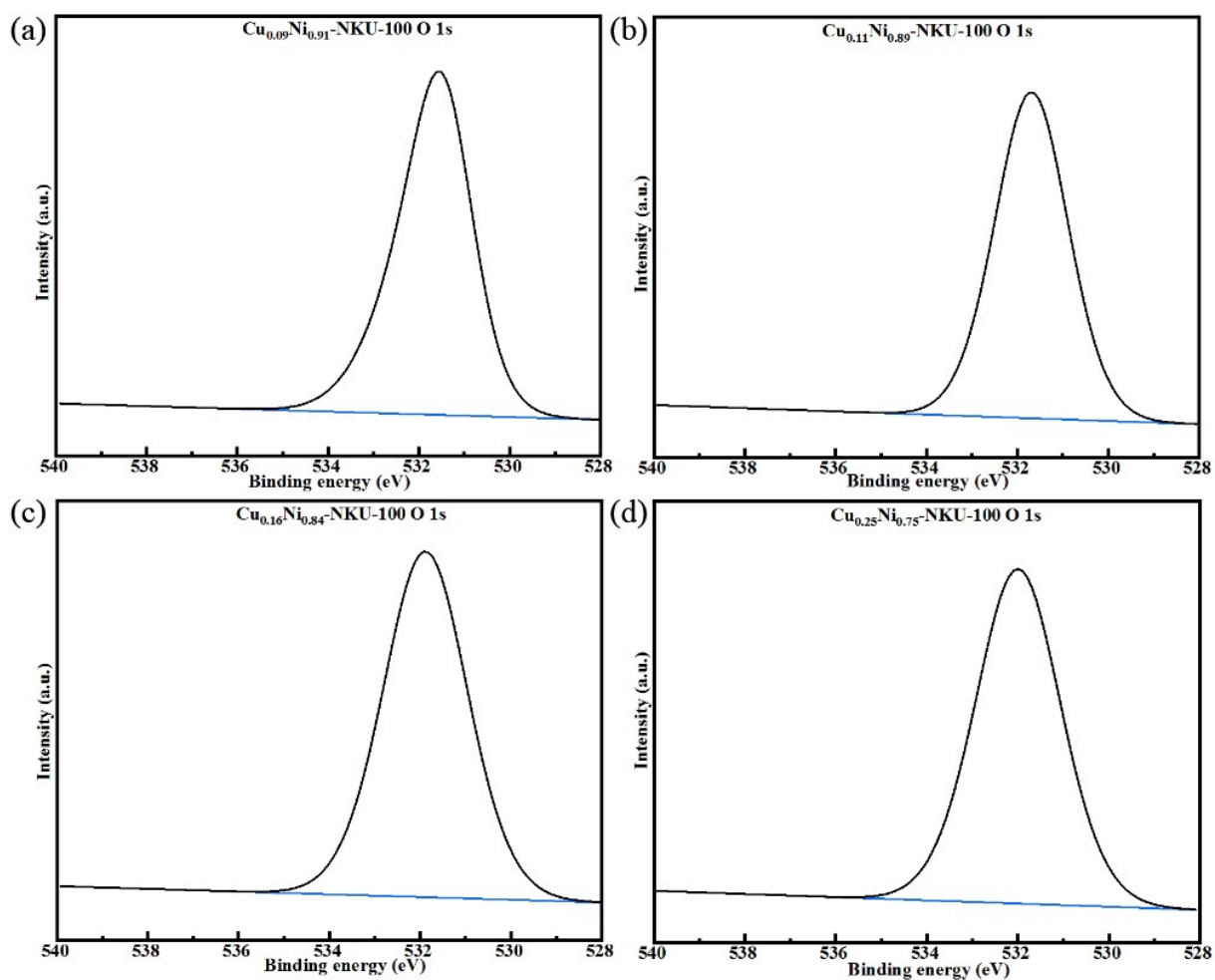


Fig. S12 High-resolution XPS of O 1s for (a) $\text{Cu}_{0.09}\text{Ni}_{0.91}\text{-NKU-100}$, (b) $\text{Cu}_{0.11}\text{Ni}_{0.89}\text{-NKU-100}$, (c) $\text{Cu}_{0.16}\text{Ni}_{0.84}\text{-NKU-100}$ and (d) $\text{Cu}_{0.25}\text{Ni}_{0.75}\text{-NKU-100}$.

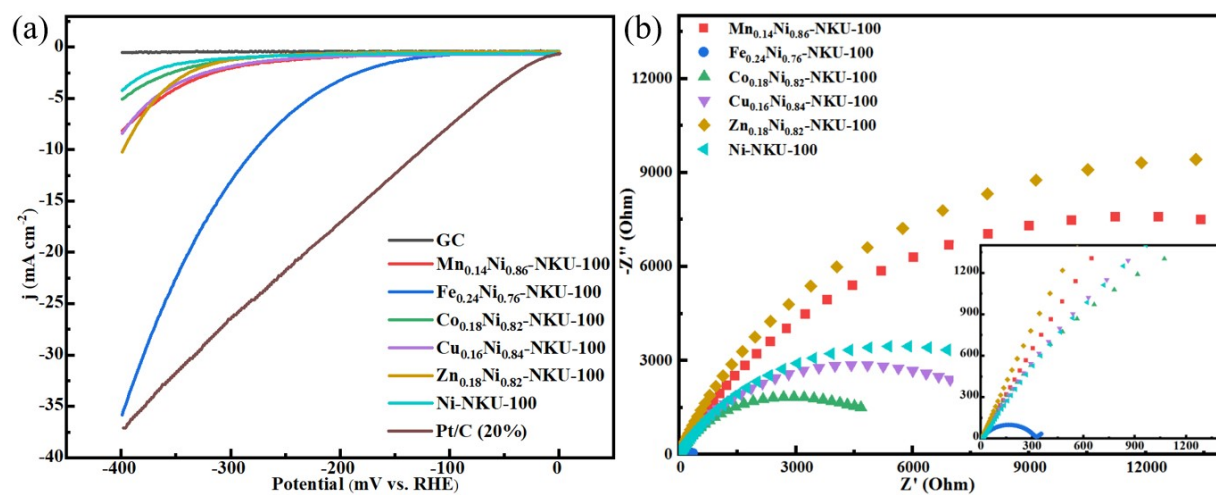


Fig. S13 (a) LSV curves at a scan rate of 5 mV·s⁻¹ and (b) EIS Nyquist plots of M_xNi_{1-x}-NKU-100 (M = Mn, Fe, Co, Cu, Zn) in 1 M NaOH electrolyte.

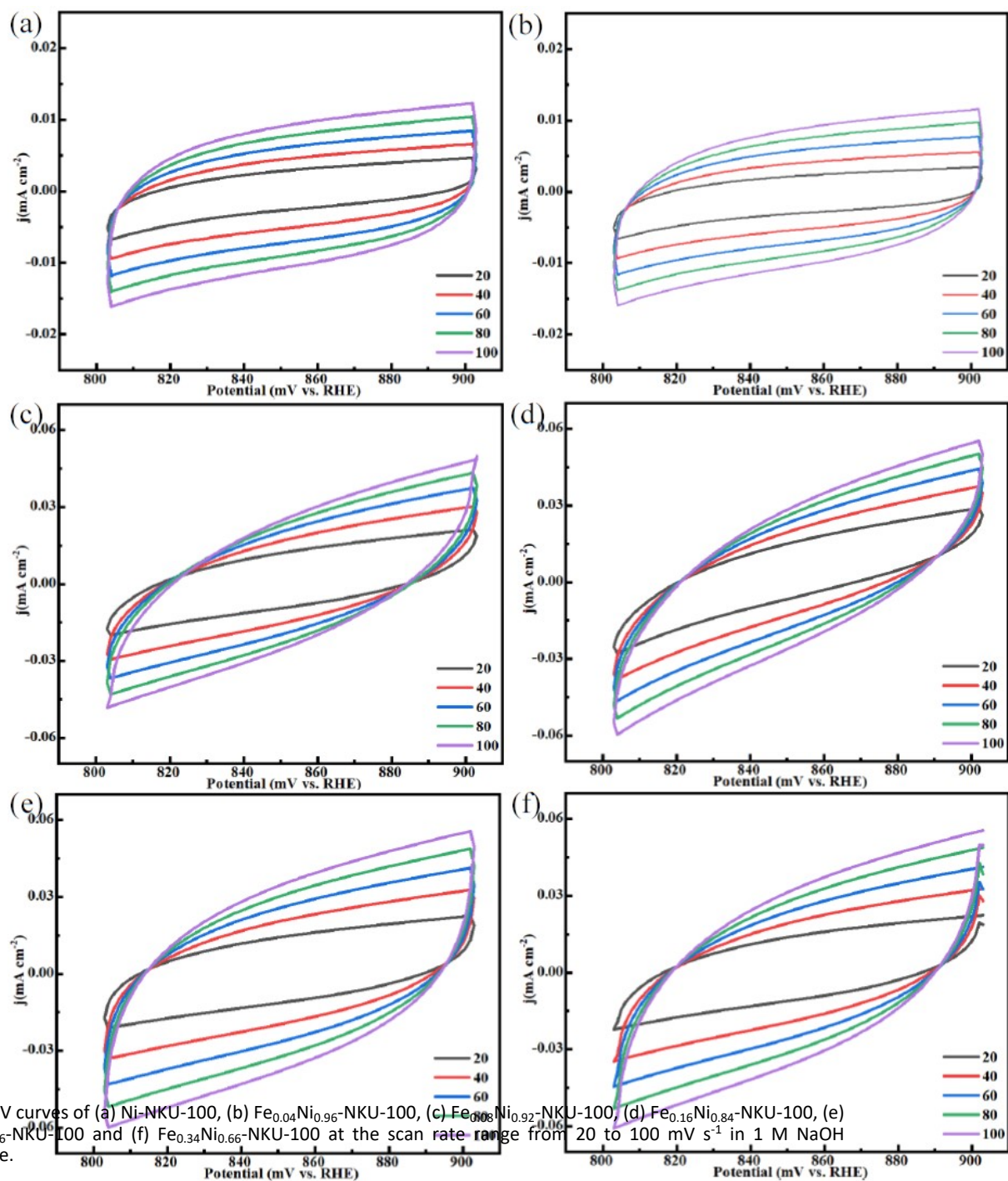


Fig. S14 CV curves of (a) Ni-NKU-100, (b) $\text{Fe}_{0.04}\text{Ni}_{0.96}$ -NKU-100, (c) $\text{Fe}_{0.08}\text{Ni}_{0.92}$ -NKU-100, (d) $\text{Fe}_{0.16}\text{Ni}_{0.84}$ -NKU-100, (e) $\text{Fe}_{0.24}\text{Ni}_{0.76}$ -NKU-100 and (f) $\text{Fe}_{0.34}\text{Ni}_{0.66}$ -NKU-100 at the scan rate range from 20 to 100 mV s^{-1} in 1 M NaOH electrolyte.

Tab. S4 R_{ct} of $\text{Fe}_x\text{Ni}_{1-x}$ -NKU-100 in 1 M NaOH electrolyte.

Electrode material	R_{ct} (Ω)
Ni-NKU-100	35070
$\text{Fe}_{0.04}\text{Ni}_{0.96}$ -NKU-100	2115
$\text{Fe}_{0.08}\text{Ni}_{0.92}$ -NKU-100	577
$\text{Fe}_{0.16}\text{Ni}_{0.84}$ -NKU-100	410
$\text{Fe}_{0.24}\text{Ni}_{0.76}$ -NKU-100	204
$\text{Fe}_{0.34}\text{Ni}_{0.66}$ -NKU-100	809

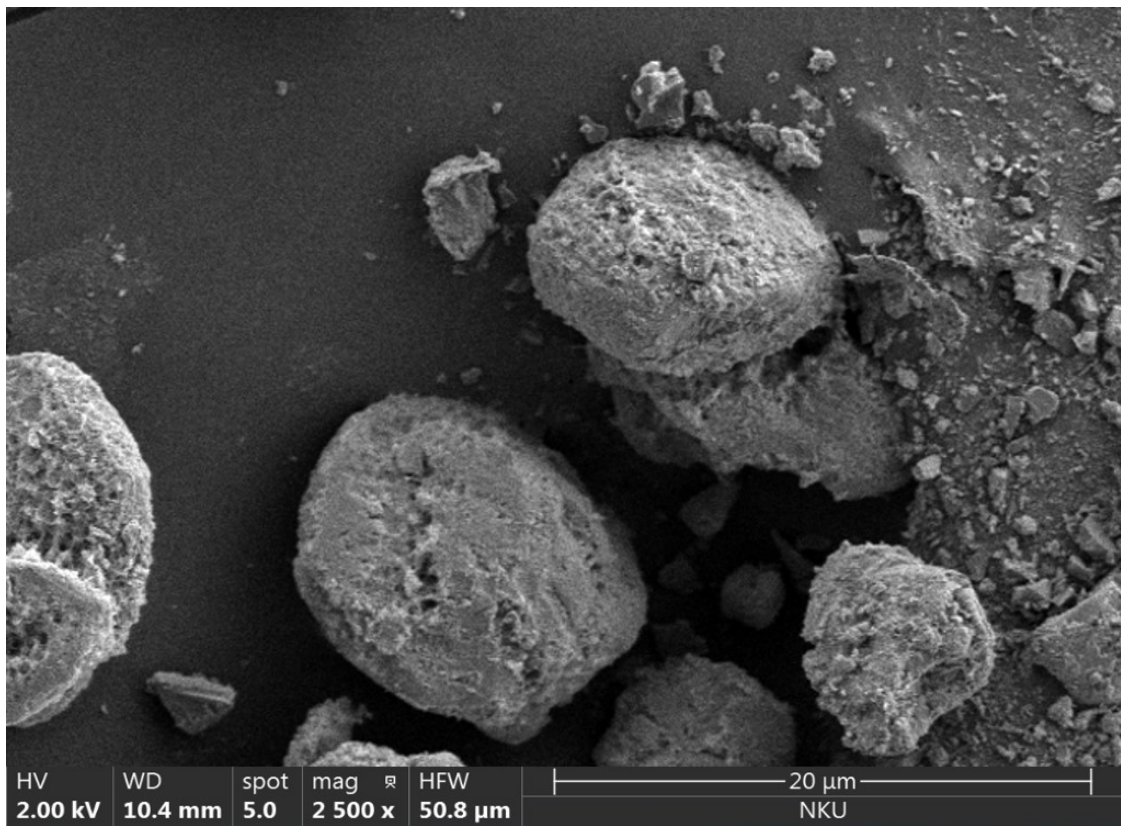


Fig. S15 SEM images of $\text{Fe}_{0.24}\text{Ni}_{0.76}\text{-NKU-100}$ after long-time electrocatalytic test in 1 M NaOH electrolyte.

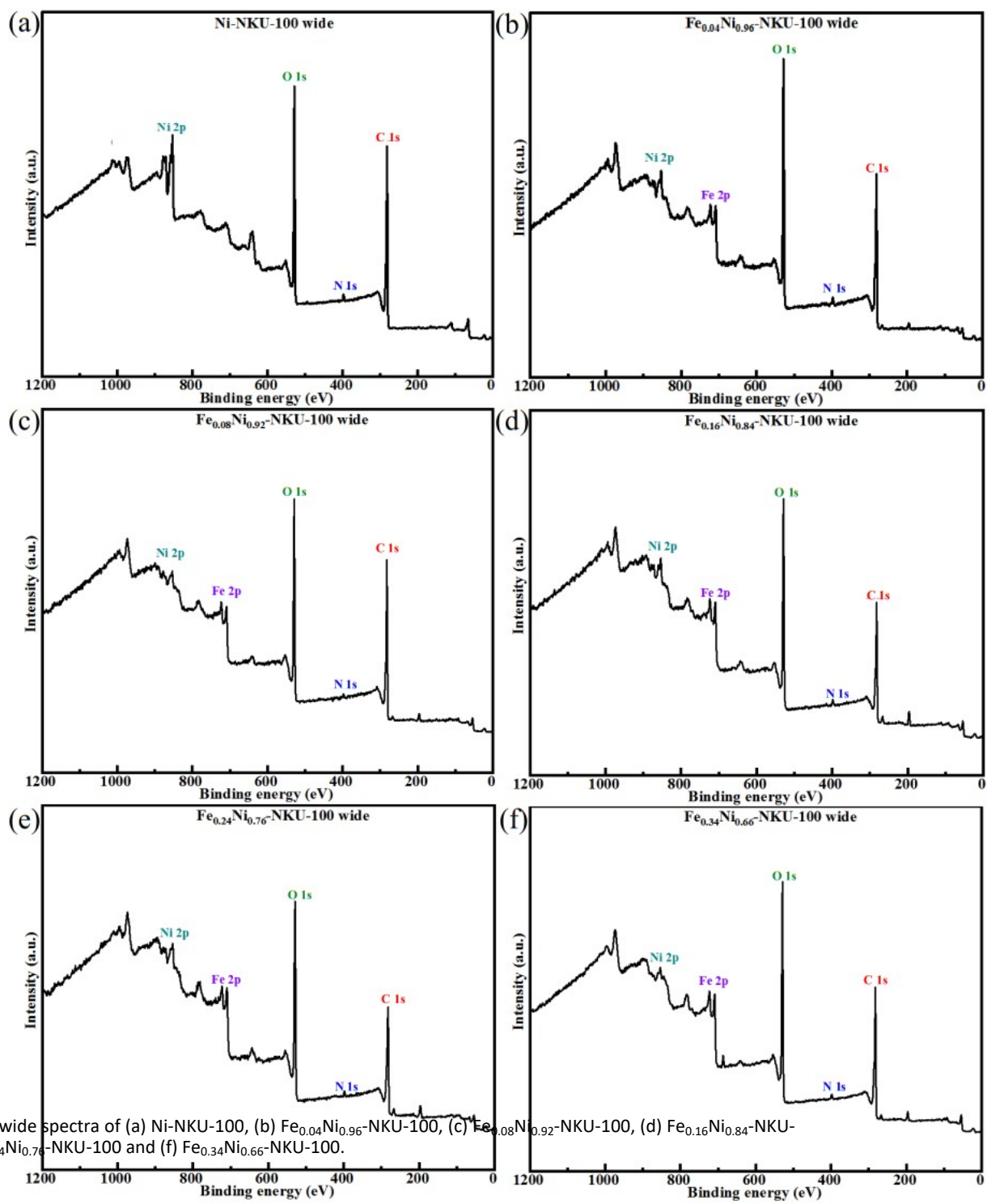


Fig. S16 XPS wide spectra of (a) Ni-NKU-100, (b) $\text{Fe}_{0.04}\text{Ni}_{0.96}$ -NKU-100, (c) $\text{Fe}_{0.08}\text{Ni}_{0.92}$ -NKU-100, (d) $\text{Fe}_{0.16}\text{Ni}_{0.84}$ -NKU-100, (e) $\text{Fe}_{0.24}\text{Ni}_{0.76}$ -NKU-100 and (f) $\text{Fe}_{0.34}\text{Ni}_{0.66}$ -NKU-100.

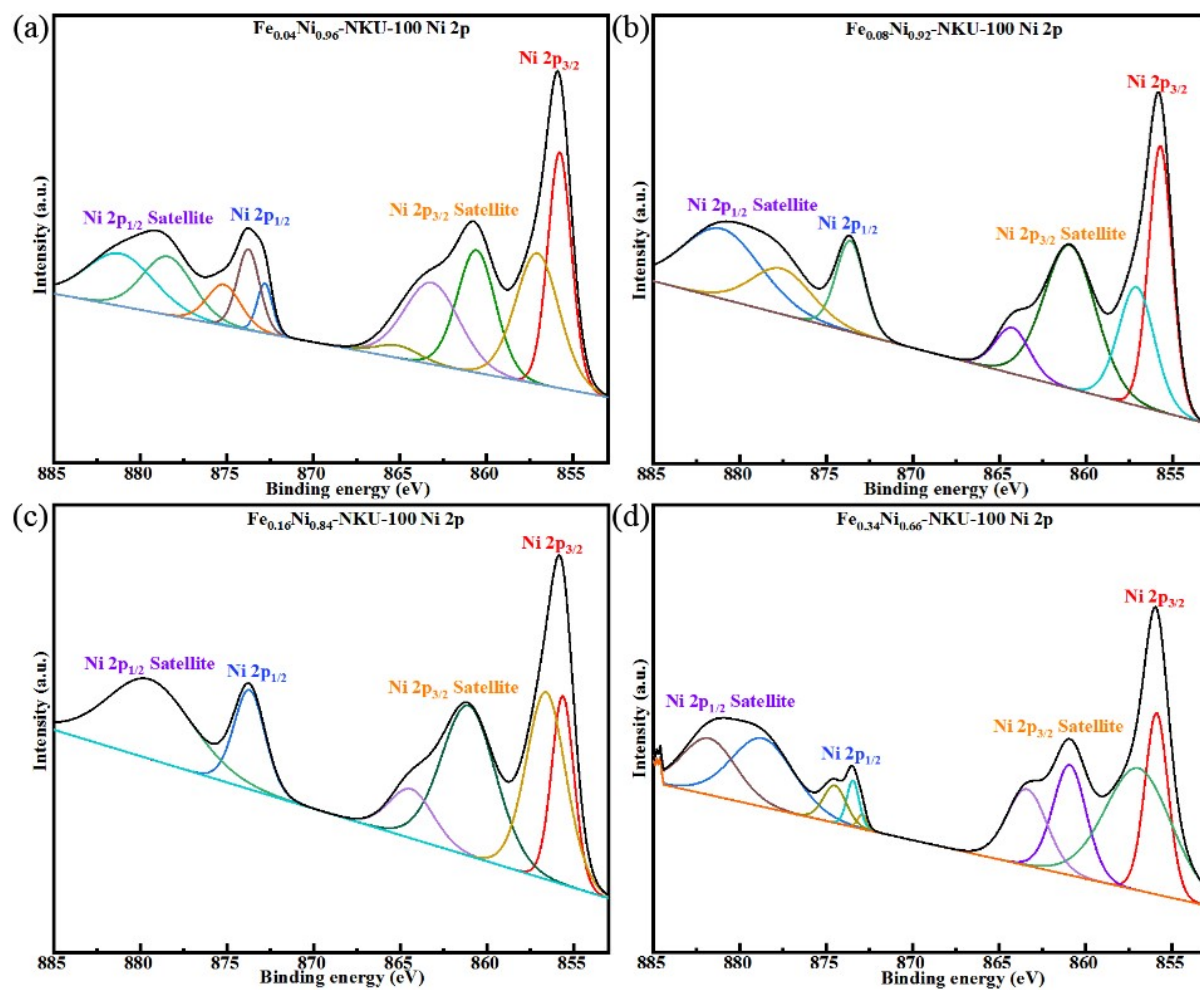


Fig. S17 High-resolution XPS of Ni 2p for (a) Fe_{0.04}Ni_{0.96}-NKU-100, (b) Fe_{0.08}Ni_{0.92}-NKU-100, (c) Fe_{0.16}Ni_{0.84}-NKU-100 and (d) Fe_{0.34}Ni_{0.66}-NKU-100.

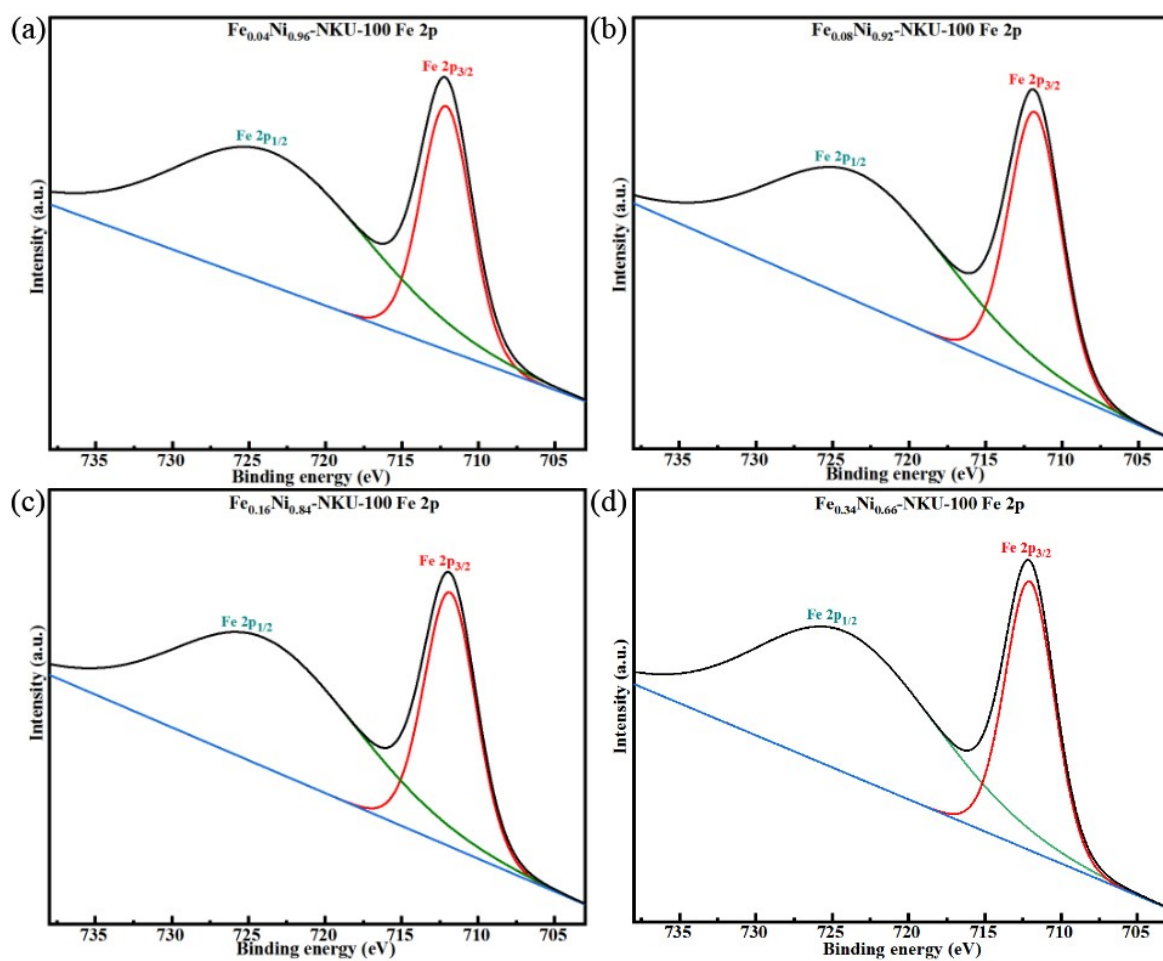


Fig. S18 High-resolution XPS of Fe 2p for (a) $\text{Fe}_{0.04}\text{Ni}_{0.96}\text{-NKU-100}$, (b) $\text{Fe}_{0.08}\text{Ni}_{0.92}\text{-NKU-100}$, (c) $\text{Fe}_{0.16}\text{Ni}_{0.84}\text{-NKU-100}$ and (d) $\text{Fe}_{0.34}\text{Ni}_{0.66}\text{-NKU-100}$.

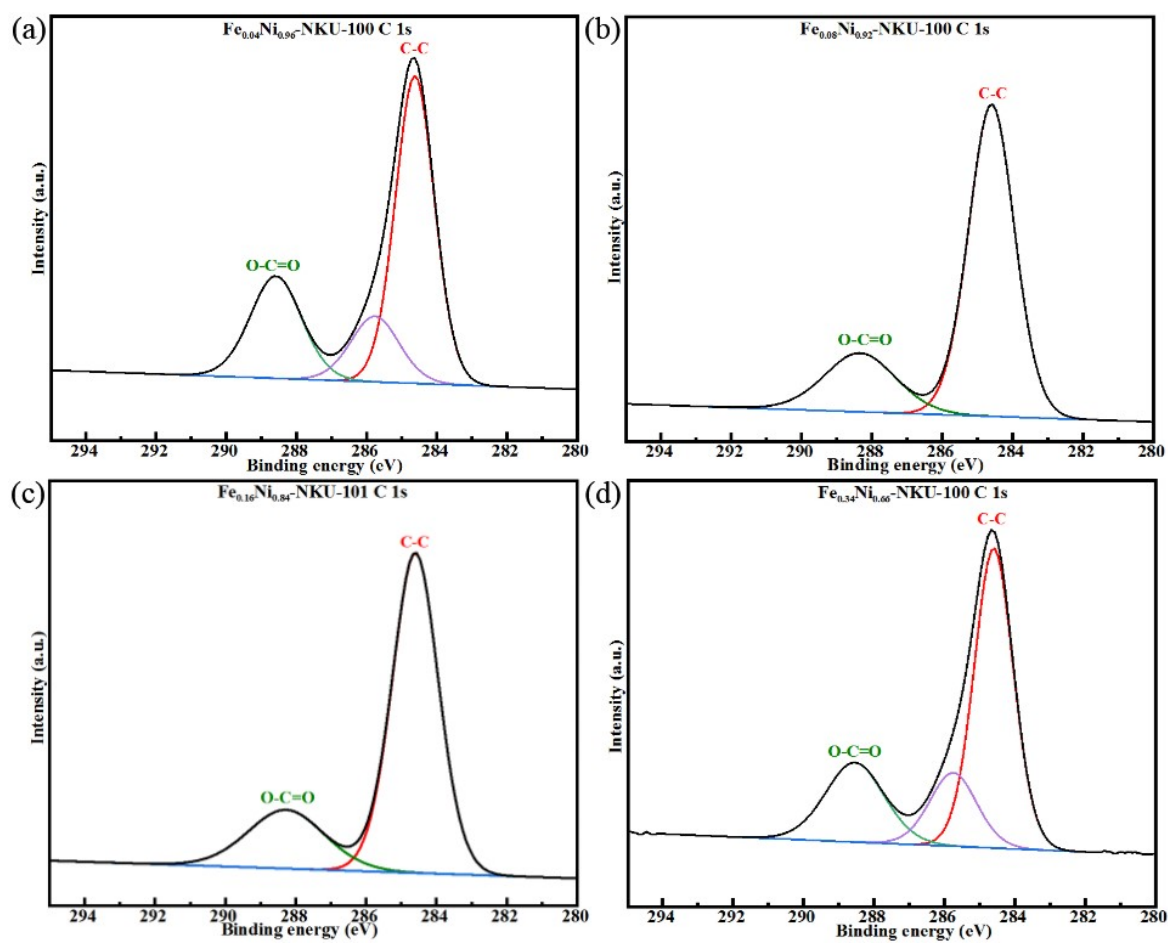


Fig. S19 High-resolution XPS of C 1s for (a) $\text{Fe}_{0.04}\text{Ni}_{0.96}\text{-NKU-100}$, (b) $\text{Fe}_{0.08}\text{Ni}_{0.92}\text{-NKU-100}$, (c) $\text{Fe}_{0.16}\text{Ni}_{0.84}\text{-NKU-101}$ and (d) $\text{Fe}_{0.34}\text{Ni}_{0.66}\text{-NKU-100}$.

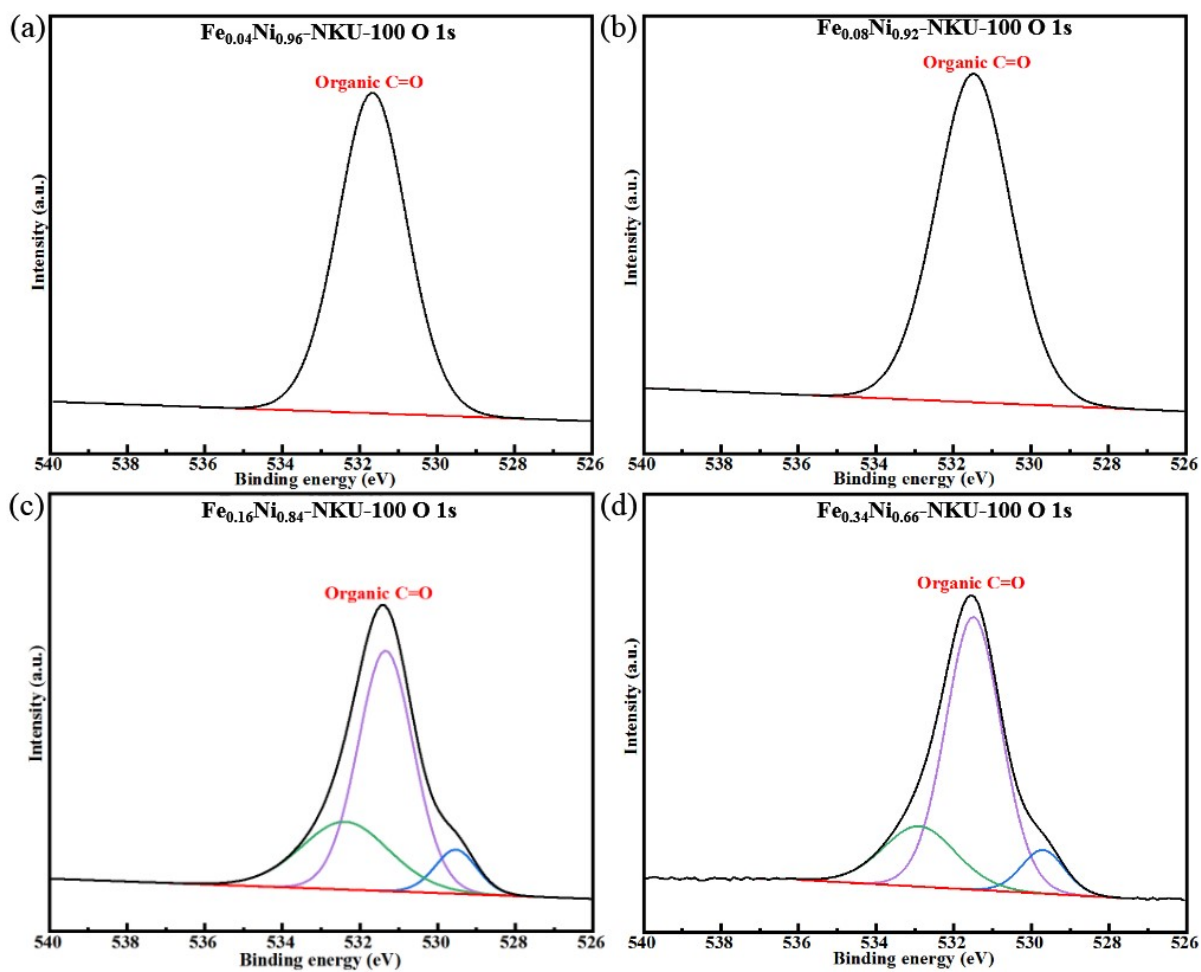


Fig. S20 High-resolution XPS of O 1s for (a) $\text{Fe}_{0.04}\text{Ni}_{0.96}\text{-NKU-100}$, (b) $\text{Fe}_{0.08}\text{Ni}_{0.92}\text{-NKU-100}$, (c) $\text{Fe}_{0.16}\text{Ni}_{0.84}\text{-NKU-100}$ and (d) $\text{Fe}_{0.34}\text{Ni}_{0.66}\text{-NKU-100}$.

References

- 1 X. Wang, J.Y. Luo, J.W. Tian, D.D. Huang, Y.P. Wu, S. Li and D.S. Li, Two new 3D isostructural Co/Ni-MOFs showing four-fold polyrotaxane-like networks: Synthesis, crystal structures and hydrogen evolution reaction, *Inorg. Chem. Comm.*, 2018, **98**, 141–144.
- 2 Y.C. Zhou, W.W. Dong, M.Y. Jiang, Y.P. Wu, D.S. Li, Z.F. Tian and J. Zhao, A new 3D 8-fold interpenetrating 66-dia topological Co-MOF: Syntheses, crystal structure, magnetic properties and electrocatalytic hydrogen evolution reaction, *J. Solid. State. Chem.*, 2019, **279**, 120929.
- 3 R. Dong, Z. Zheng, D.C. Tranca, J. Zhang, N. Chandrasekhar, S. Liu, X. Zhuang, G. Seifert and X. Feng, Immobilizing Molecular Metal Dithiolene-Diamine Complexes on 2D Metal-Organic Frameworks for Electrocatalytic H₂ Production, *Chem. Eur. J.*, 2017, **23**, 2255–2260.
- 4 W. Zhou, Y.P. Wu, X. Wang, J. Wu Tian, D.D. Huang, J. Zhao, Y.Q. Lan and D.S. Li, Improved conductivity of a new Co(II)-MOF by assembled acetylene black for efficient hydrogen evolution reaction, *CrystEngComm*, 2018, **20**, 4804–4809.
- 5 S. Roy, Z. Huang, A. Bhunia, A. Castner, A.K. Gupta, X. Zou and S. Ott, Electrocatalytic Hydrogen Evolution from a Cobaloxime-Based Metal-Organic Framework Thin Film, *J. Am. Chem. Soc.*, 2019, **141**, 15942–15950.
- 6 R. Dong, M. Pfeiffermann, H. Liang, Z. Zheng, X. Zhu, J. Zhang and X. Feng, Large-area, Free-Standing, Two-Dimensional Supramolecular Polymer Single-Layer Sheets for Highly Efficient Electrocatalytic Hydrogen Evolution, *Angew. Chem. Int. Ed.*, 2015, **54**, 12058–12063.
- 7 D.H. He, J.J. Liu, Y. Wang, F. Li, B. Li and J.B. He, Electrocatalysis of the first electron transfer in hydrogen evolution reaction with an atomically precise Cu^{II}-organic framework catalyst, *Electrochim. Acta.*, 2019, **308**, 285–294.
- 8 J.S. Qin, D.Y. Du, W. Guan, X.J. Bo, Y.F. Li, L.P. Guo, Z.M. Su, Y.Y. Wang, Y.Q. Lan and H.C. Zhou, Ultrastable Polymolybdate-Based Metal-Organic Frameworks as Highly Active Electrocatalysts for Hydrogen Generation from Water, *J. Am. Chem. Soc.*, 2015, **137**, 7169–7177.
- 9 I. Hod, P. Deria, W. Bury, J.E. Mondloch, C.W. Kung, M. So, M.D. Sampson, A.W. Peters, C.P. Kubiak, O. K. Farha and J. T. Hupp, A porous proton-relaying metal-organic framework material that accelerates electrochemical hydrogen evolution, *Nat. Commun.*, 2015, **6**, 8304.
- 10 X.F. Li, M.Y. Lu, H.Y. Yu, T.H. Zhang, J. Liu, J.H. Tian and R. Yang, Copper-Metal Organic Frameworks Electrodeposited on Carbon Paper as an Enhanced Cathode for the Hydrogen Evolution Reaction, *ChemElectroChem.*, 2019, **6**, 4507–4510.
- 11 R.-Z. Zhang, L.-L. Lu, Z.-H. Chen, X. Zhang, B.-Y. Wu, W. Shi and P. Cheng, Bimetallic Cage-Based Metal-Organic Frameworks for Electrochemical Hydrogen Evolution Reaction with Enhanced Activity, *Chem. Eur. J.*, 2022, **28**, **28**, e202200401.
- 12 D. Zhu, J. Liu, Y. Zhao, Y. Zheng and S.Z. Qiao, Engineering 2D Metal–Organic Framework/MoS₂ Interface for Enhanced Alkaline Hydrogen Evolution, *Small*, 2019, **15**, 1805511.
- 13 J. Duan, S. Chen and C. Zhao, Ultrathin metal-organic framework array for efficient electrocatalytic water splitting, *Nat. Commun.*, 2017, **8**, 15341.
- 14 S.N. Shreyanka, J. Theerthagiri, S.J. Lee, Y. Yu and M.Y. Choi, Multiscale design of 3D metal–organic frameworks (M–BTC, M: Cu, Co, Ni) via PLAL enabling bifunctional electrocatalysts for robust overall water splitting, *Chem. Eng. J.*, 2022, **446**, 137045.
- 15 B. Geng, F. Yan, X. Zhang, Y. He, C. Zhu, S.-L. Chou, X. Zhang and Y. Chen, Conductive CuCo-Based Bimetal Organic Framework for Efficient Hydrogen Evolution, *Adv. Mater.*, 2021, **33**, 2106781.

- 16 W. Cheng, H. Zhang, D. Luan and X.W. (David) Lou, Exposing unsaturated Cu₁-O₂ sites in nanoscale Cu-MOF for efficient electrocatalytic hydrogen evolution, *Sci. Adv.*, 2021, **7**, eabg2580.
- 17 M. Gu, S.-C. Wang, C. Chen, D. Xiong and F.-Y. Yi, Iron-Based Metal–Organic Framework System as an Efficient Bifunctional Electrocatalyst for Oxygen Evolution and Hydrogen Evolution Reactions, *Inorg. Chem.*, 2020, **59**, **9**, 6078–6086.
- 18 H. Huang, Y. Zhao, Y. Bai, F. Li, Y. Zhang and Y. Chen, Conductive Metal–Organic Frameworks with Extra Metallic Sites as an Efficient Electrocatalyst for the Hydrogen Evolution Reaction, *Adv. Sci.*, 2020, **7**, 2000012.